Use of CFRP to Maintain Composite Action for Continuous Steel–Concrete Composite Girders

Alfarabi M. Sharif[1]; Mohammad A. Samaaneh[2]; Abul K. Azad[3]; and Mohammed H. Baluch[4]

Abstract: The loss of composite action at the negative moment region for a continuous composite girder reduces the girder's strength and stiffness. This paper presents an experimental investigation into the use of carbon fiber–reinforced polymer (CFRP) to maintain the composite action at the negative moment region of continuous composite girders. This is achieved by bonding CFRP sheets to the top of a concrete slab at the negative moment region. Six two-span continuous composite girders were tested. CFRP sheet thickness was varied to assess its effect on girder behavior. The girders were designed to have full composite action between the concrete slab and the steel girder. Moment capacity at the positive and negative moment regions was evaluated experimentally and theoretically. A plastic analysis was conducted to evaluate the ultimate capacity of the girders. Finite-element modeling evaluated girder performance numerically. The experimental results confirmed the effectiveness of CFRP sheets in maintaining composite action at the negative moment region and in preventing crack initiation in a concrete slab under service load. The use of CFRP improved the strength and stiffness of the continuous composite girders. The plastic analysis safely estimated the girders' ultimate capacity. The developed finite-element model yielded satisfactory results. **DOI: 10.1061/(ASCE)CC.1943-5614.0000645.** © *2015 American Society of Civil Engineers.*

Author keywords: Carbon fiber–reinforced polymer (CFRP); Composite action; Continuous composite girders; Structural strengthening.

Introduction

Continuous composite steel–concrete girders composed of cast-in-place concrete slabs and steel girders are widely used in bridges and buildings. In design, the concrete slab at the negative moment region is ignored for composite action because of tensile stress, and the steel girder is assumed to act alone or compositely with the longitudinal slab reinforcement (AISC 2005). The inactivity of the slab in composite action at the negative moment regions diminishes the full composite action of the girders, resulting in reduced strength and stiffness.

Researchers have used internal and external prestressing techniques to overcome the loss of composite action at the negative moment regions of continuous composite girders. Basu et al. (1987b, a) partially prestressed concrete slabs at the negative moment region for two-span continuous composite girders. The concrete slab was cast in two stages. In the first stage, the slab was cast at the negative moment region. Then prestressing force was directly applied to the slab so that it would act compositely with the steel girder. In the second stage, the rest of the concrete slab covering the positive moment regions was cast. Chen et al. (2009) used external prestressing for two- and three-span continuous composite girders. The continuous composite girders were prestressed by external tendons attached to the steel girders. Both prestressing techniques successfully maintained the composite action at the negative moment regions for service load and improved girder strength and stiffness. The recent development of CFRP offers an attractive solution for strengthening structures. Several researchers have used CFRP to improve concrete and steel girder strength. Galal et al. (2011) strengthened a simple-span steel beam with CFRP sheets and obtained strength and stiffness improvements. Continuous-span steel beams were investigated by Kadhim (2012). CFRP plates were bonded to the bottom steel flange at the mid-span to improve beam capacity. A simple-span composite steel–concrete girder was bonded by CFRP sheets to the bottom surface of the bottom steel flange by Tavakkolizadeh et al. (2003). Siddiqui (2010) and Aravind et al. (2013) conducted extensive research on strengthening concrete structures using CFRP sheets; both reported that CFRP was effective in increasing the ultimate capacity of concrete structures.

In view of limited published work on the use of CFRP to strengthen composite girders at the negative moment zone, the authors conducted experiments to evaluate the effectiveness of CFRP in providing composite action at this zone. The aim of this paper is to present the findings of these experiments, in which a CFRP sheet was bonded to the top of a concrete slab at the negative moment region for two-span continuous composite girders; structural performance was evaluated up to failure. A theoretical evaluation using plastic analysis determined the girders' ultimate capacity. Finally, girder behavior was evaluated numerically via finite-element modeling using the commercial software *ABAQUS*.

Experimental Program

Details of the two-span continuous composite girders tested in this program are shown in Fig. 1. The built-up steel section was proportioned to eliminate any secondary failure, including local buckling, web yielding, web crippling, and lateral torsional buckling. The girders were designed to develop full composite action between the girder and the concrete slab using 19-mm-diameter shear studs

[1]Professor, King Fahd Univ. of Petroleum and Minerals, Dhahran 31261, Saudi Arabia (corresponding author). E-mail: fmsharif@kfupm.edu.sa

[2]Ph.D. Student, King Fahd Univ. of Petroleum and Minerals, Dhahran 31261, Saudi Arabia. E-mail: samaaneh@kfupm.edu.sa

[3]Professor, King Fahd Univ. of Petroleum and Minerals, Dhahran 31261, Saudi Arabia. E-mail: akazad@kfupm.edu.sa

[4]Professor, King Fahd Univ. of Petroleum and Minerals, Dhahran 31261, Saudi Arabia. E-mail: mhbaluch@kfupm.edu.sa

Note. This manuscript was submitted on May 6, 2015; approved on September 21, 2015; published online on December 30, 2015. Discussion period open until May 30, 2016; separate discussions must be submitted for individual papers. This paper is part of the ***Journal of Composites for Construction***, © ASCE, ISSN 1090-0268.

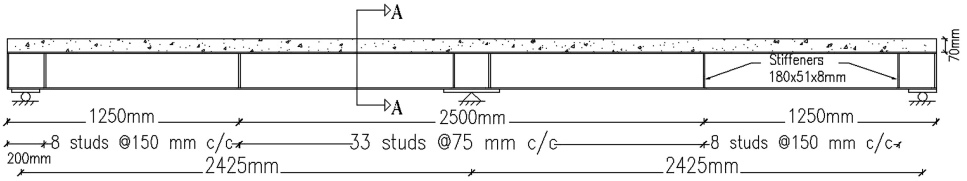

Fig. 1. Two-span continuous composite girder dimensions

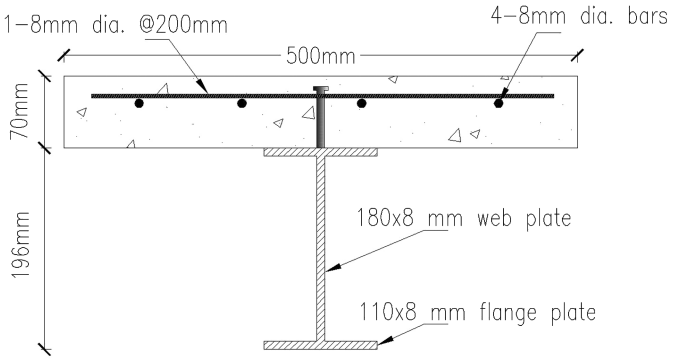

Fig. 2. Girder Section A-A, cross section details

Table 1. Girder Matrix

Group	Girder	CFRP thickness (mm)	Concrete slab wrapped with CFRP at positive moment region
1	RG	—	No
	G1	0.131	
	G2	0.262	
	G3	0.393	
2	RGR	—	Yes
	G2R	0.262	

embedded to a length of 50 mm in the slab. The cross section dimensions for the girders are shown in Fig. 2.

A total of six composite girders were fabricated and cast. In the first phase, four girders, RG, G1, G2, and G3 (Table 1), were tested to evaluate the effectiveness of CFRP at the negative moment region, as shown in Fig. 3. Girder RG, fabricated without CFRP, was used as the control, and Girders G1, G2, and G3 had varying thicknesses of CFRP bonded to the top of the concrete slab (Fig. 3). The CFRP length was established in accordance with ACI 313-08 (ACI 2008), including development length. When tested, all four girders developed concrete slab shear-compression failure at the positive moment region. For more enhancement of ultimate strength and utilization of CFRP at the negative moment region, two additional girders, RGR and G2R (Table 1), making up Group 2, were tested by wrapping the their slabs with CFRP at the positive moment region, as shown in Fig. 4, to prevent shear-compression failure. The RGR girder without CFRP at the negative moment region was the control for Group 2, and Girder G2R had CFRP bonded to the top of its concrete slab at the negative moment region. In other words, Girder RGR had wrapping at the positive moment region and Girder G2R had both CFRP wrapping at the positive moment region and a bonded CFRP sheet at the negative moment region. The CFRP thickness used for the girder was the same as that used for Girder G2 of Group 1.

Materials

The mechanical properties of concrete are given in Table 2, and the concrete compressive stress-strain is shown in Fig. 5. The mechanical properties of the structural steel and steel reinforcement are listed in Table 3 and their stress-strain is shown in Figs. 6 and 7, respectively. The CFRP used was Grade-230 Nitowrap FRC (Fosroc Company, London, U.K.) of 0.131-mm thickness and 500-mm sheet width. The design tensile strength of a single dry CFRP sheet was 3,483 MPa, its ultimate strain was 0.015, and its elastic modulus was 232,200 MPa.

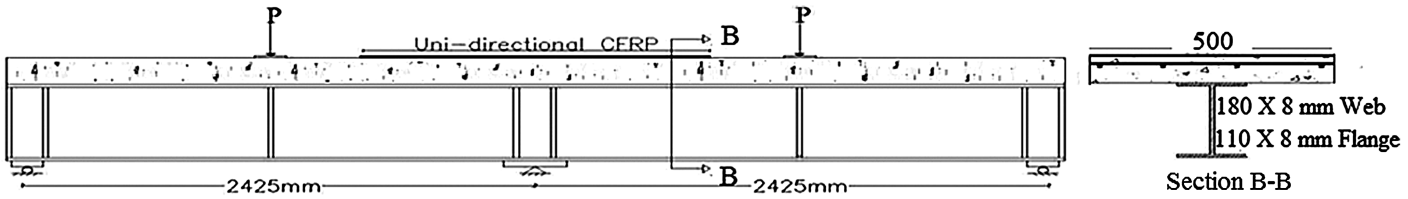

Fig. 3. Composite girder bonded with CFRP at the negative moment region

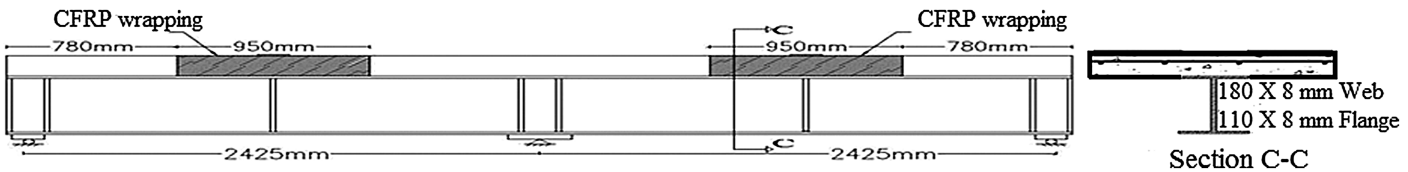

Fig. 4. Composite girder wrapped with CFRP at the mid-span

Table 2. Concrete Mechanical Properties

Property	Design value
Compressive strength for cylinders (MPa)	26.4
Young's modulus (MPa)	23,800
Poisson's ratio	0.2
Strain at ultimate load	0.0028
Strain at failure	0.0037

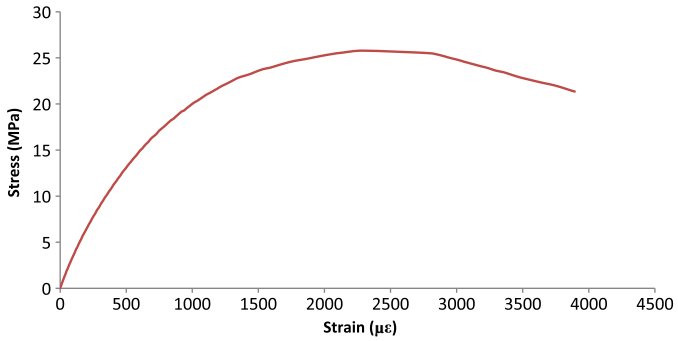

Fig. 5. Concrete compression stress-strain

Table 3. Steel and Steel Reinforcement Mechanical Properties

Material	Yield strength (MPa)	Ultimate strength (MPa)	Yield strain	Modulus of elasticity (MPa)	Poisson's ratio
Structural steel	278.6	430.7	0.0014	205,000	0.291
Steel reinforcement	417.7	601.3	0.00205	205,000	0.301

Nitowrap primer base and Nitowrap hardener, mixed according to the manufacturer's specifications, was used as the epoxy adhesive for bonding the CFRP sheet. The shear strength of the adhesive was evaluated by a pullout test (Bilotta 2010). The CFRP sheet was bonded to the concrete block as shown in Fig. 8. Strain gauges were fixed to the CFRP sheet surface to measure slip between the sheet and the concrete block. The load versus slip curve for the adhesive is shown in Fig. 9. The adhesive shear strength was 2.0 MPa and behaved elastically up to 1.4 MPa.

The shear capacity of the studs was evaluated by a two-way push-out test (Topkaya et al. 2004). A steel section with two shear

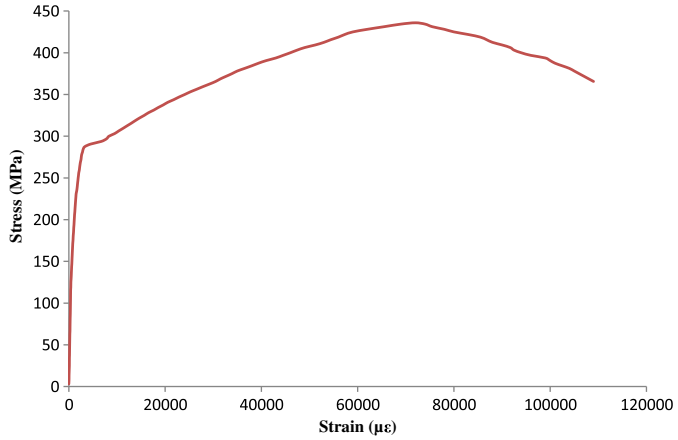

Fig. 6. Structural steel tensile stress-strain

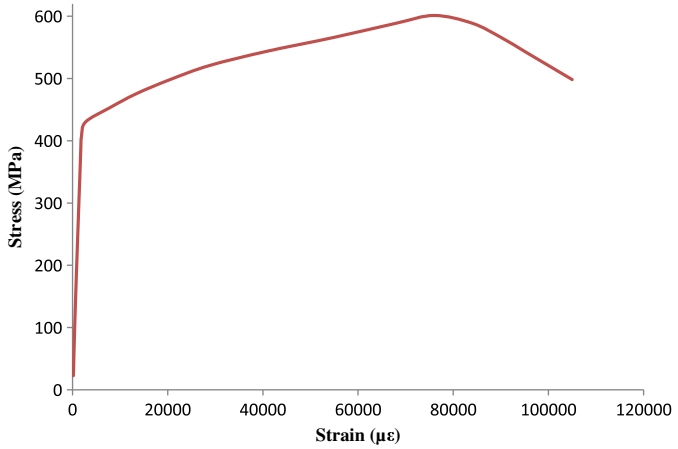

Fig. 7. Steel reinforcement tensile stress-strain

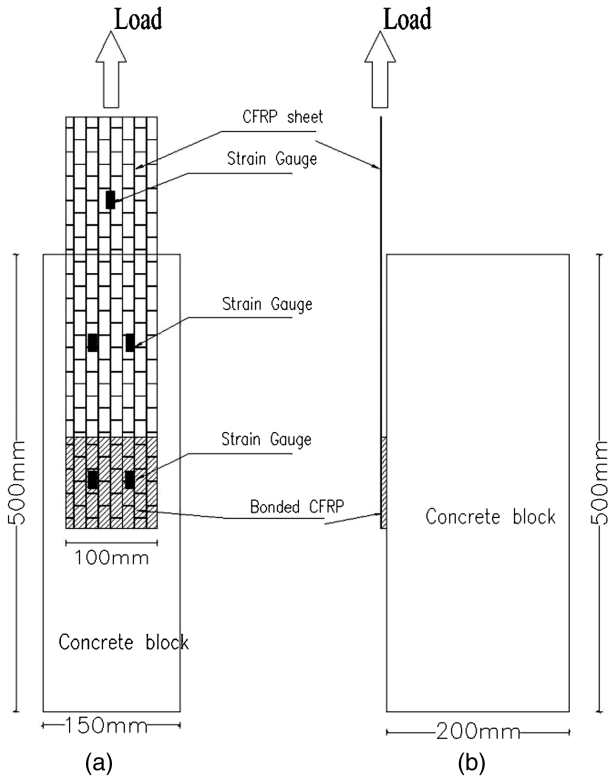

Fig. 8. Pull-out test for adhesive: (a) front view; (b) side view

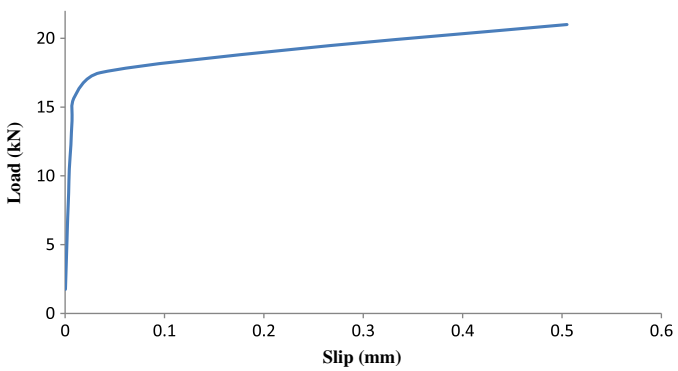

Fig. 9. Load–slip curve for interface of CFRP, adhesive, and concrete

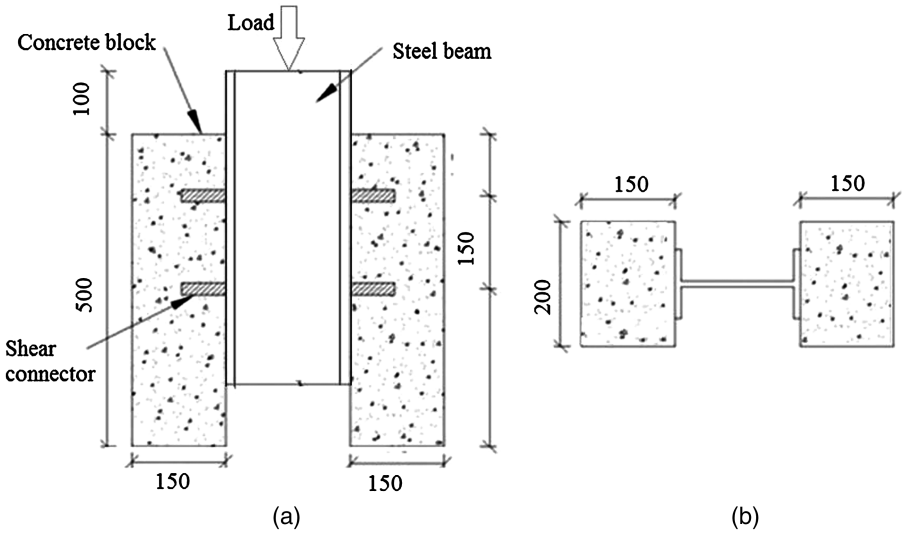

Fig. 10. Two-way-push-out test for shear studs: (a) side view; (b) top view

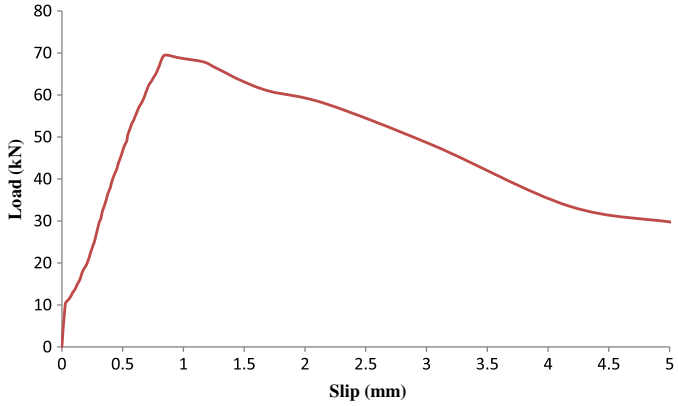

Fig 11. Load–slip curve for interface of steel girder, shear studs, and concrete slab

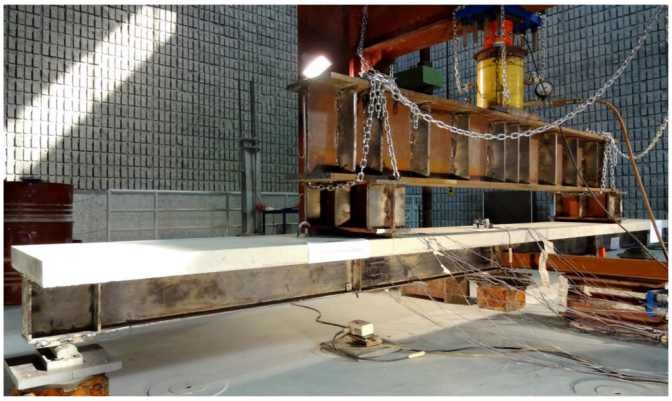

Fig. 12. Tested continuous composite girder

studs at each side was cast with concrete as shown in Fig. 10. A LVDT was fixed at the bottom of the steel section to measure the slip and load applied at the top of the steel section. The measured load versus shear connector slip is shown in Fig. 11.

Test Setup and Instrumentation

Concrete surfaces were roughened and cleaned by removing the surface laitance and ensuring that the surfaces were dry, flat, and sound before the CFRP fabrics were bonded to the concrete slab. The epoxy adhesive was applied to cover the prepared concrete surfaces. The fabrics were then firmly applied to the concrete slab and left to cure for one week before testing.

All girders were tested under five-point bending with the compression flange over the interior support laterally supported, as shown in Fig. 12. The girders were loaded at a rate of 1.0 kN/s to failure.

Strain gauges were mounted on the steel section, steel reinforcement, concrete slab, and CFRP fabrics, as shown in Fig. 13. The deflection at the mid span at each loading step was recorded using a LVDT, which was fixed to the bottom of the concrete slab over the interior support and at the midspan to measure slip between the concrete slab and the steel girder at these locations. In addition, one LVDT was used at the top of the concrete slab over the interior support to measure crack width.

Experimental Results and Discussion

Cracking Load and Yield Load

Cracking load, P_{cr}, is defined as load-initiating cracks visible in the concrete slab over the interior support caused by tensile stress from bending. Yielding load, P_y, is defined as the upper limit of the service load at which yielding of the girder's bottom flange at the midspan occurs. The ratio of cracking load to yielding load, λ, is taken as the indicator of the level at which the composite action should be maintained at the negative moment region under service load. This is to prevent premature cracking of the slab. Higher values of λ indicate a higher load level at which cracking occurs. The values of P_{cr} and P_y, recorded from test observations, are shown in Table 4 along with values of λ. The girders with CFRP bonded to the top of the concrete slab at the negative moment region, G1, G2, G3, and G2R, exhibited considerably higher P_{cr} and λ values than the control girders, RG and RGR. This clearly confirms that the proposed

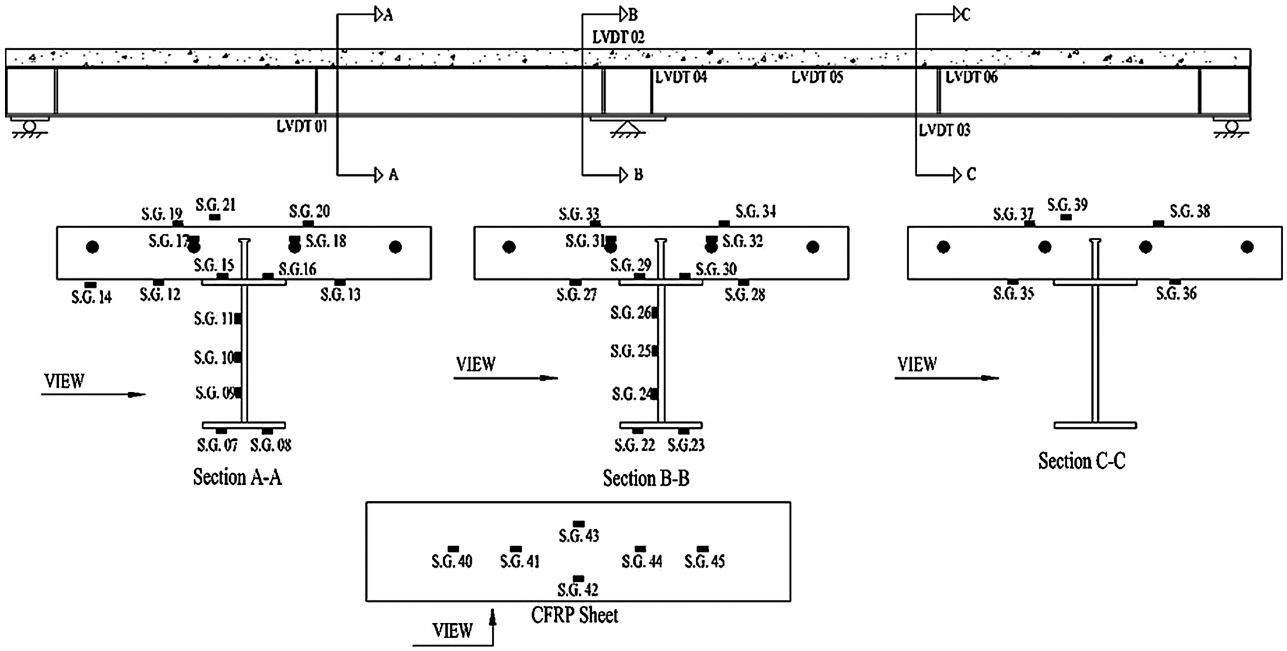

Fig. 13. Strain gauge (S.G.) and LVDT locations

Table 4. Girder Cracking Load, Yielding Load, and Ratio of Cracking Load to Yielding Load

Group	Girder	P_{cr} (kN)	P_y (kN)	λ
1	RG	77	163	0.47
	G1	123	165	0.75
	G2	136	173	0.79
	G3	150	175	0.86
2	RGR	65	172	0.38
	G2R	150	182	0.82

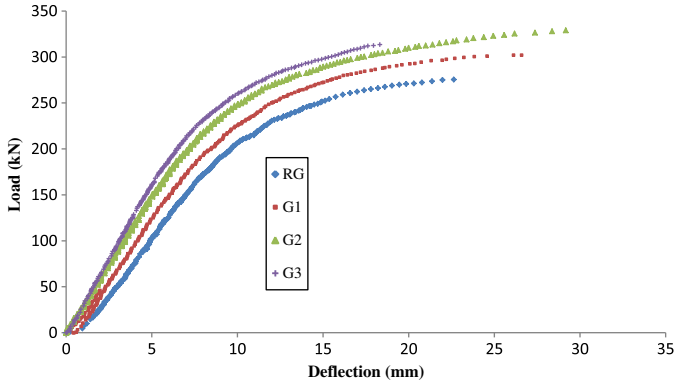

Fig. 14. Group-1 load deflection curve

strengthening maintains composite action at the negative moment region at a load level closer to the maximum service load.

Composite Girder Behavior

All girders exhibited linear and nonlinear behavior, as noted from the load deflection plots shown in Fig. 14. Nonlinear behavior occurred soon after the load caused tension yielding of the bottom flange plate at the mid-span. Improvement in girder strength and stiffness due to CFRP inclusion is observed in Fig. 14.

Table 5. Correspondence of Load and Steel Section Yielding (kN)

Girder	Yielding of bottom flange (mid-span)	Yielding of bottom flange (interior support)	Yielding of top flange (interior support)
RG	163	228	240
G1	165	225	255
G2	173	222	260
G3	175	249	263

The loads corresponding to flange plate yielding at the mid-span and at the interior support, as observed from the strain measurements, are listed in Table 5 for Girders RG, G1, G2, and G3. The yield load at the mid-span, corresponding to the bottom flange-plate yielding, is lower than the load-caused yielding of the bottom flange plate at the support because of the upward shift of the neutral axis at the mid-span due to full composite action. At a load, P, higher than the yield load (e.g., 228 kN for RG), the yielding part of the beam section experienced strain hardening (Fig. 6), causing the section to rotate inelastically at the interior support. The resulting bending moment distribution for the girders was influenced by a major increase in the positive moment and only a marginal increase in the negative moment. The use of CFRP produced only a small change in yield load (Table 5), although it increased P_u considerably (Fig. 14).

The inelastic rotation of the girders at the support was due to post-yield loading caused by yielding of the significant part of the steel section, as evidenced by the measured strains at the ultimate load (Figs. 15 and 16). The linear strain lines best fit the measured values.

Ultimate Moment Capacity

Based on the measured strains, the moment capacities of the girders at positive moment locations (M_{+ve}) and negative moment

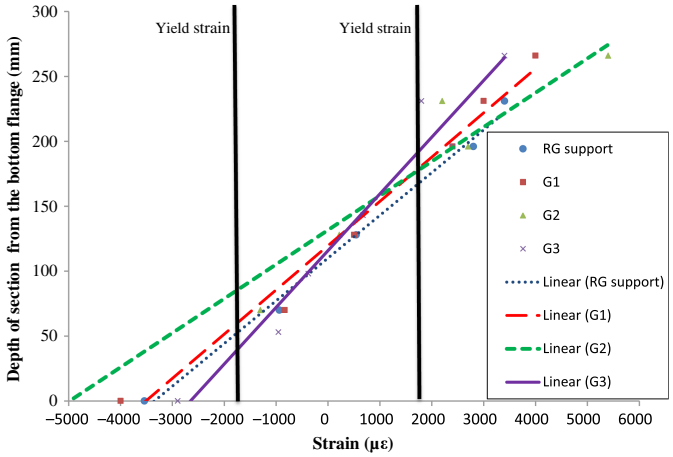

Fig. 15. Group I strain distribution at the interior support at ultimate load

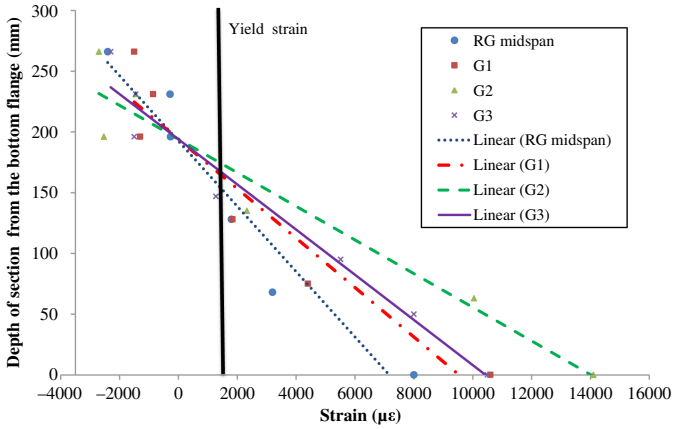

Fig. 16. Group 1 strain distribution at the mid-span at ultimate load

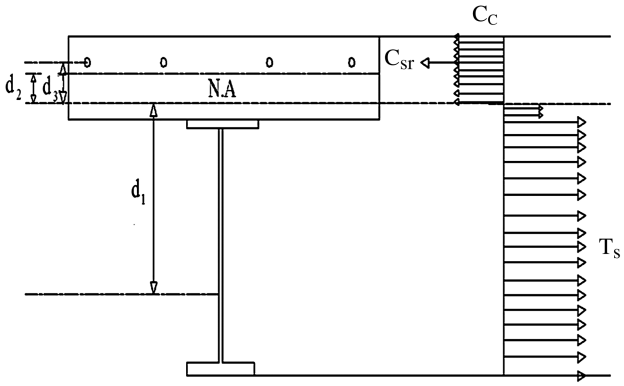

Fig. 17. Stress distribution at the positive moment region at ultimate load

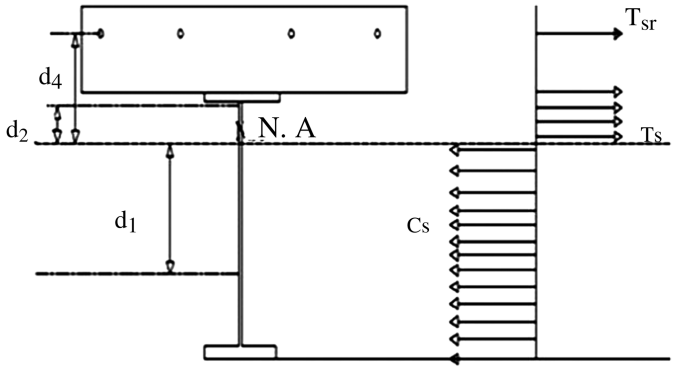

Fig. 18. Stress distribution at the negative moment region at ultimate load

locations ($M_{-\text{ve}}$ for RG, $M^*_{-\text{ve}}$ for G1, G2, and G3) were calculated and are listed in Table 6.

Theoretical values for girder ultimate positive and negative moment capacities were calculated as follows, assuming the stress distributions shown in Figs. 17–19, which corresponded to the elastic-plastic behavior of the steel without strain hardening:

$$\breve{M}_{+\text{ve}} = T_s(d_1) + C_c(d_2) + C_{S.R}(d_3) \quad (1)$$

$$\breve{M}_{-\text{ve}} = C_s(d_1) + T_{S.R}(d_4) + T_s(d_2) \quad (2)$$

$$\breve{M}^*_{-\text{ve}} = C_s(d_1) + T_{S.R}(d_4) + T_s(d_2) + T_{\text{CFRP}}(d_3) \quad (3)$$

Eq. (2) includes the contribution of the slab's longitudinal reinforcing bars in composite action. Eq. (3) applies to girders having CFRP glued to the top of the concrete slab at the negative moment region. In Eqs. (1)–(3), T_s and C_s are the tension and compression forces in the steel section, respectively, C_c is the compression force in the concrete, $T_{S.R}$ and $C_{S.R}$ are the tension and compression forces in the steel reinforcement, respectively, and T_{CFRP} is the tension force in the CFRP sheets corresponding to an assumed maximum tensile stress 0.3 times the ultimate CFRP tensile strength. This level of stress was selected to ensure yielding of both steel flanges and limit CFRP stress due to rupture failure in this material.

Theoretical values for moment capacities $\breve{M}_{+\text{ve}}$ and $\breve{M}_{-\text{ve}}$ for all girders were calculated using Eqs. (1)–(3) and are shown in Table 6. Because of composite action at the positive moment region, the $\breve{M}_{+\text{ve}}$ values were higher than the $\breve{M}_{-\text{ve}}$ values. The addition of CFRP increased the negative moment capacity, reducing the ratio $\breve{M}_{+\text{ve}}/\breve{M}_{-\text{ve}}$ from 1.49 for the Control Girder, RG, to 1.05 for Girder G3. As for Girder G3, the thickness of the CFRP yielded

Table 6. Expected Capacity at Positive and Negative Moment Zones and Corresponding Loads

Girder	$\breve{M}_{+\text{ve}}$ (kN · m)	$\breve{M}_{-\text{ve}}$ or $\breve{M}^*_{-\text{ve}}$ (kN · m)	α_p	$\breve{P}_{tf}$ (kN)	M_{+ve} (kN · m)	$M_{-\text{ve}}$ or $M^*_{-\text{ve}}$ (kN · m)	α_e	P_{tf} (kN)	P_u (kN)
RG	110	74	1.49	243	112	76	1.48	248	273
G1	110	84	1.31	250	112	86	1.30	256	303
G2	110	90	1.22	256	120	95	1.26	276	330
G3	110	104	1.05	267	111	93	1.19	260	314

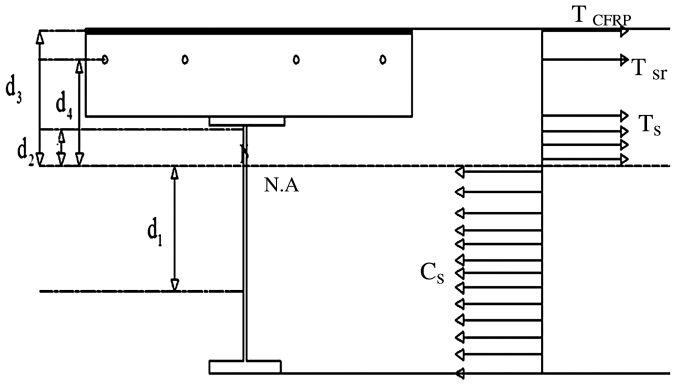

Fig. 19. Stress distribution at the negative moment region at ultimate load with CFRP

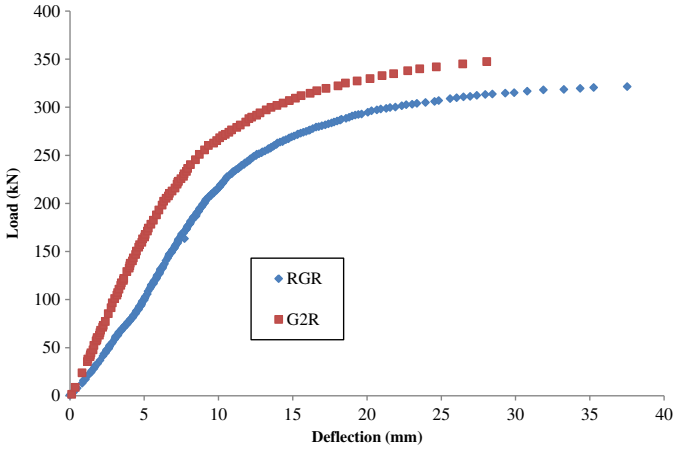

Fig. 20. Group-2 girder load deflection curves

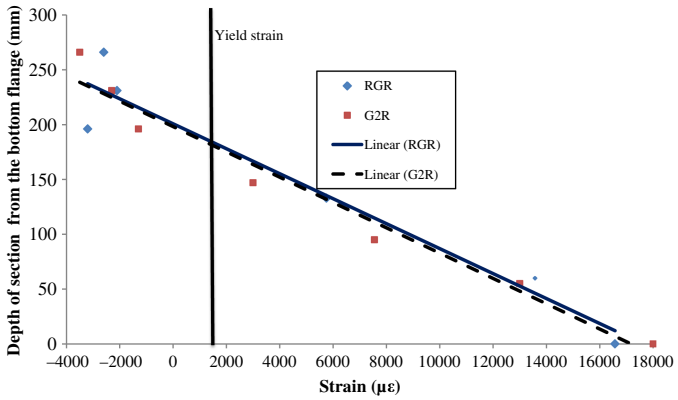

Fig. 21. Group 2 strain distribution at the mid-span at ultimate load

almost equal-strength $\check{M}_{+ve}$ and $\check{M}^{*}_{-ve}$. Apparently this was the theoretical CFRP upper limit in this case. The values for failure load P_u for the girders are shown in Table 6.

Plastic Analysis

The values of P_u were compared with those determined from plastic analysis and from the measured strain along the girder depth at positive and negative moment locations. Using plastic analysis, the theoretical maximum value of load P necessary to cause failure is given as

$$P = \left[\frac{2(2\alpha + 1)Mp}{L}\right] \tag{4}$$

where M_p = negative moment capacity; and α = ratio of positive to negative moment capacity.

The values of α are listed in Table 6 as α_p for the plastic moment capacities and as α_e for the experimentally determined moment capacities from the measured strain. Using α_p and α_e, the corresponding values of failure load P are calculated from Eq. (3) and are shown in Table 6 as $\check{P}_{tf}$ and P_{tf}. Because the strain in the girders was measured at locations 200 mm away from the mid-span and the centerline of the interior support, strain values were slightly lower than those at the maximum moment locations. Consequently, the measured values of M_{-ve} *and* M_{+ve} were lower than the values corresponding to the strains at the maximum positive and negative moment locations.

Table 6 shows that the analytical values calculated assuming full yielding of the sections were lower than the experimental values P_u and P_{tf} for all girders that developed proper rotation at the interior support. The experimental ultimate load P was higher than the calculated failure load for all girders—even Girder G3, which did not develop the plastic capacity of the steel section at the interior support. This means that the calculated failure load $\check{P}_{tf}$ was a safe estimate of the actual failure load, which becomes higher as the steel girder surpasses its excess capacity because of strain hardening.

Slab Confinement at the Positive Moment Regions

Because all girders failed at the mid-span as a result of slab failure, leaving the negative moment region structurally intact, it was of interest to determine if load-carrying capacity could be further enhanced by preventing slab failure at the mid-span. As stated earlier, in two Group-2 girders, RGR and G2R, the slab was wrapped with CFRP. Tests confirmed that an additional increase in load capacity was achieved. The confinement of the concrete slab increased the ultimate load to 321 kN for Girder RGR compared with 273 kN for Girder RG. The CFRP increased the ultimate load capacity to 348 kN. The load deflection plot in Fig. 20 shows the enhancement in load capacity and stiffness.

Confining the concrete slab at the mid-span allowed the steel section over the interior support to undergo relatively more rotation compared with the girders in Group 1. Linear strain lines that best fit the measured strain for the mid-span and interior support locations are shown in Figs. 21 and 22, respectively. They clearly demonstrate that a substantial part of the steel section yielded at both locations. The strain distribution along the cross section at the mid-span shows that both RGR and G2R developed almost the full capacity of the section. At the negative moment region, the steel section of Girder RGR yielded almost entirely compared with the partial yielding of the steel section for G2R. This was because of different failure types. However, the yielding part of the steel section of Girder G2R at the negative moment region was greater in size than the yielding parts of the steel sections of Group-1 girders.

Variations in CFRP Thickness

The effect of CFRP thickness on the behavior of Girders G1, G2, and G3 is shown in Fig. 12. As observed, girder strength and stiffness improvements were directly proportional to increases in CFRP

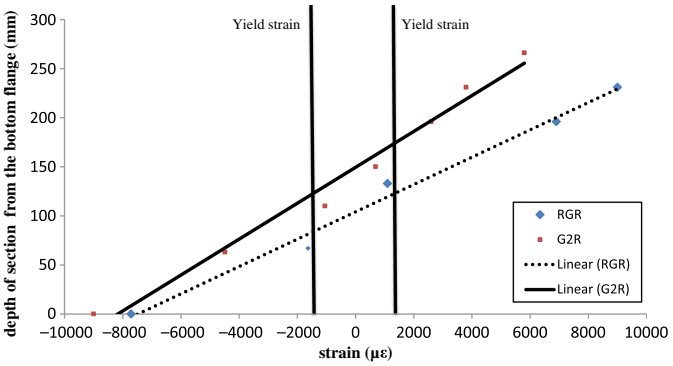

Fig. 22. Group 2 strain distribution at the interior support at ultimate load

Fig. 23. Girder G1 shear compression failure

Fig. 24. Girder RGR concrete slab crushing at the mid-span

thickness. Girder G3 showed minimal strength and stiffness improvement relative to Girder G2. The increase in CFRP thickness for Girder G3 increased the ultimate negative moment capacity close to the positive moment capacity (Table 6). This caused less girder rotation at the interior support and girder failure at the mid-span before reaching the moment capacity at the negative moment region. Consequently, Girder G3 recorded a smaller failure load P_u compared with girder G2.

Failure Modes

All Group-I girders failed because of concrete slab shear compression at the positive moment region, as shown in Fig. 23. The stress at the top of the concrete slab under the point load at this stage was approximately $0.85f_c$ according to the strain measurements. The

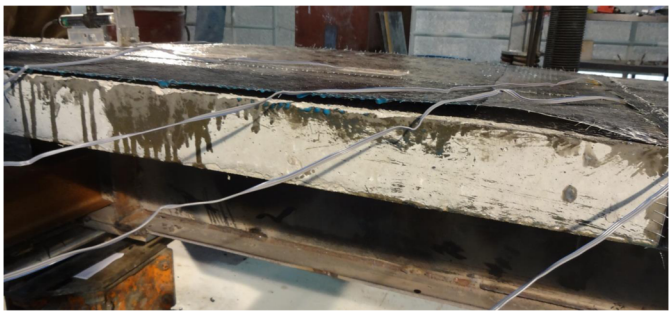

Fig. 25. Girder G2R CFRP debonding

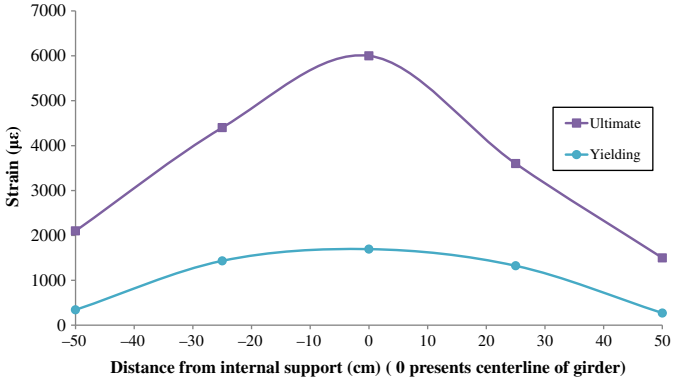

Fig. 26. Girder G2R CFRP longitudinal strain at the negative moment region

Group-2 control girder, RGR, reached its capacity with the crushing of the concrete slab at the positive moment region, as captured in Fig. 24, after removal of the CFRP sheet. The strain measurements at the top of the concrete indicated that the ultimate strength of the slab at ultimate load was exceeded. Girder G2R failed prematurely because of debonding of the CFRP fabrics over the interior support, as shown in Fig. 25. The transferred shear force due to the CFRP over the interior support at failure was 188 kN, which caused shear stress at the interface between the concrete and the CFRP that exceeded the epoxy adhesives' ultimate strength of 2 MPa.

CFRP Strain Measurements

Strain measurements along the CFRP fabrics at the negative moment region were used to assess the CFRP's contribution to load resistance at different load levels. They showed that CFRP strain decreased a little as CFRP thickness increased. This was because the increase in thickness caused an upward shift of the neutral axis. However, the CFRP strain increased sharply after both steel flanges yielded at the interior support, and the final CFRP strain is controlled by the level of rotation at that section. Measured strains in CFRP fabrics occurred at the interior support, as expected. A sudden increase in measured strain was noticed at locations where concrete slab cracking took place, as shown in Fig. 26.

Finite-Element Modeling

A nonlinear finite-element model was developed using the commercial software program *ABAQUS*. Two-span continuous composite girders were modeled using the *ABAQUS/Explicit*

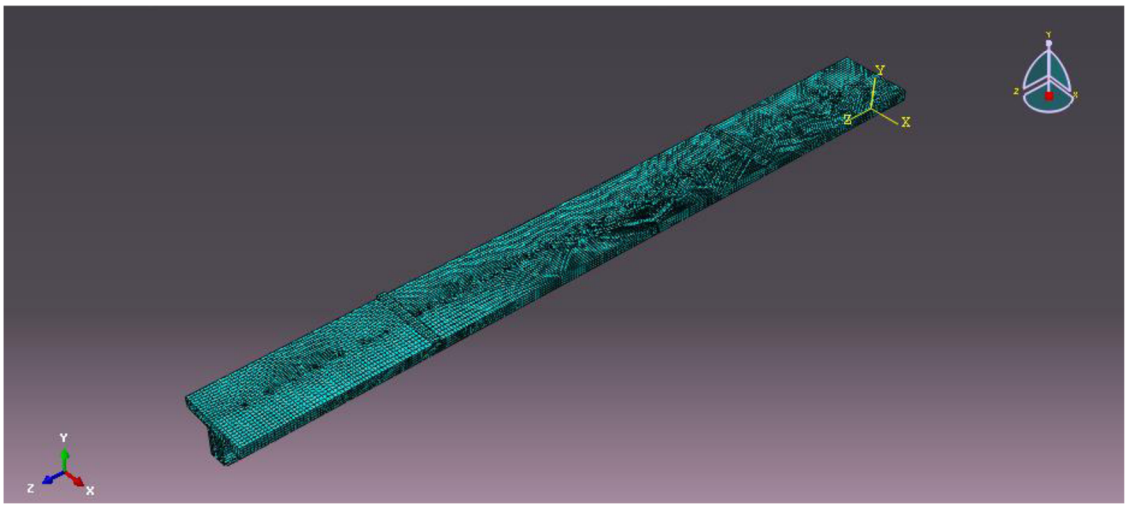

Fig. 27. Modeled girder mesh size

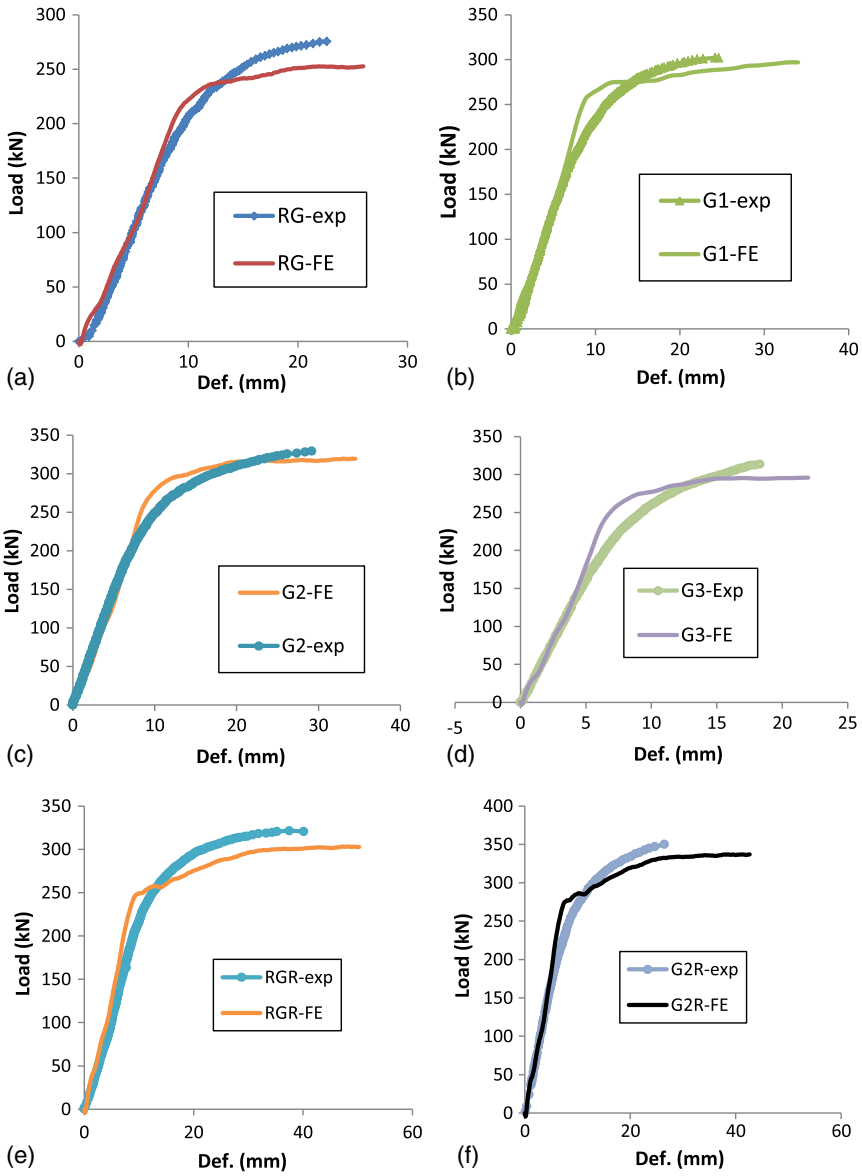

Fig. 28. Comparison of numerical and experimental load deflection curves: (a) Girder RG; (b) Girder G1; (c) Girder G2; (d) Girder G3; (e) Girder RGR; (f) Girder G2R

solver. Point loads were applied as two equivalent pressure loads on the 50-mm-wide bearing steel mounted on top of the concrete slab and covered its full width. One pin and two roller line restraints were assigned in the middle of the bearing plates at the supports. The composite girder components were meshed on a part-by-part basis. A regular structured hex-dominated mesh was generated, and an adequate mesh size was adopted. The concrete slab, steel section, and shear studs were modeled using an eight-node linear brick element (C3D8R); steel reinforcement was modeled using a two-node linear 3D truss (T3D2); and a four-node doubly curved thin or thick shell (S4R) was used to model the CFRP.

The concrete was modeled using an isotropic plasticity model and a concrete damage plasticity model. The latter employed the yield function proposed by Lubliner et al. (1989) and later modified by Lee and Fenves (1998) and followed a nonassociated flow rule. The plasticity model required the input data from Fig. 5. Structural steel and steel reinforcement were modeled by an isotropic plasticity model using the stress-strain curves shown in Figs. 6 and 7. The CFRP was modeled as a linear elastic composite laminate with 0.131-mm thickness for each layer used. The modulus of elasticity of the matrix (CFRP and primer) used for material definition was 232,000 MPa.

Surface–surface contact was used to define the concrete–steel interaction. Mechanical interaction between the studs and the concrete surfaces was modeled using friction formulation in the tangential direction. The studs were defined as the master whereas the concrete slab was defined as the slave. The penalty method was used for tangential behavior along with a coefficient of friction of 0.2, and the maximum shear stress was specified according to the load–slip curve shown in Fig. 11. Cohesive contact was used to simulate the behavior of the adhesive material between the concrete and the CFRP sheet. The tangential stiffness was calculated from the load–slip curve shown in Fig. 9. The model allowed debonding of the CFRP sheet if the adhesive capacity was exceeded.

Numerical Results

An adequate mesh size of hexa-dominated mesh was used to obtain numerical results with adequate accuracy, as shown in Fig. 27. Experimental and numerical results for the load deflection curves shown in Fig. 28 were compared for all Group-1 and Group-2 girders. The similarity in plots with reasonable agreement lends itself to confidence in the finite-element modeling of the composite girder. The model is capable of identifying premature failures in Groups 1 and 2. The developed model can be used in a parametric study.

Conclusions

An experimental investigation of six continuous composite girders reinforced with CFRP was conducted. Testing was carried out on two groups of girders using CFRP at the negative moment region. Based on the findings of this work, the following conclusions are drawn:

- The use of CFRP sheets bonded to the top of a concrete slab at the negative moment region maintains composite action at loads close to the service load;
- Girder capacity and stiffness increase with the use of CFRP sheets bonded to the top of the concrete slab at the negative moment region; the increase in ultimate capacity is directly proportional to CFRP thickness up to certain thickness, when the negative moment capacity is close to the positive moment capacity;
- Tests showed that the theoretical prediction of failure load using plastic analysis yields values lower than the actual failure load value because of the higher load-carrying capacity of the steel girders due to strain hardening; thus, plastic analysis is safe for failure load prediction; and
- The proposed finite-element model of the continuous composite girder bonded with CFRP at the negative moment region yields satisfactory results comparable with experimental data and so can be adopted with confidence.

Acknowledgments

Financial support for this work, provided by King Fahd University of Petroleum and Minerals and the Deanship of Scientific Research under project number IN121053, is gratefully acknowledged.

References

ABAQUS version 6.13-1 [Computer software]. Dassault Systèmes, Waltham, MA.

ACI (American Concrete Institute) and ISO. (2008). "Building code requirements for structural concrete and commentary." ACI 318-08, Farmington Hills, MI.

AISC. (2005). *Manual*, 13th Ed., Chicago.

Aravind, N., Samanta, A. K., Roy, D. S., and Thanikal, J. V. (2013). "Retrofitting of reinforced concrete beams using fibre reinforced polymer (FRP) composites: A review." *J. Urban Environ. Eng.*, 7(1), 164–175.

Basu, P. K., Sharif, A. M., and Ahmed, N. U. (1987a). "Partially prestressed composite beams. II." *J. Struct. Eng.*, 10.1061/(ASCE)0733-9445(1987)113:9(1926), 1926–1938.

Basu, P. K., Sharif, A. M., and Ahmed, N. U. (1987b). "Partially prestressed continuous composite beams. I." *J. Struct. Eng.*, 10.1061/(ASCE)0733-9445(1987)113:9(1909), 1909–1925.

Bilotta, A. (2010). "Behavior of FRP-to-concrete interface: Theoretical models and experimental results." Ph.D. dissertation, Universta degli Studi di Naploi Federico II, Italy.

Chen, S., Wang, X., and Jia, Y. (2009). "A comparative study of continuous steel-concrete composite beams prestressed with external tendons: Experimental investigation." *J. Constr. Steel Res.*, 65(7), 1480–1489.

Galal, K., Seif ElDin, H. M., and Tirca, L. (2011). "Flexural performance of steel girders retrofitted using CFRP materials." *J. Compos. Constr.*, 10.1061/(ASCE)CC.1943-5614.0000264, 265–276.

Kadhim, M. M. A. (2012). "Effect of CFRP plate length strengthening continuous steel beam." *Constr. Build. Mater.*, 28(1), 648–652.

Lee, J., and Fenves, G. L. (1998). "Plastic-damage model for cyclic loading of concrete structures." *J. Eng. Mech.*, 10.1061/(ASCE)0733-9399(1998)124:8(892), 892–900.

Lubliner, J., Oliver, J., Oller, S., and Onate, E. (1989). "A plastic-damage model for concrete." *Int. J. Solids Struct.*, 25(3), 299–326.

Siddiqui, N. A. (2010). "Experimental investigation of RC beams strengthened with externally bonded FRP composites." *Lat. Am. J. Solids Struct.*, 6(4), 343–362.

Tavakkolizadeh, M., and Saadatmanesh, H. (2003). "Strengthening of steel-concrete composite girders using carbon fiber reinforced polymers sheets." *J. Struct. Eng.*, 10.1061/(ASCE)0733-9445(2003)129:1(30), 30–40.

Topkaya, C., Yura, J. A., and Williamson, E. B. (2004). "Composite shear stud strength at early concrete ages." *J. Struct. Eng.*, 10.1061/(ASCE)0733-9445(2004)130:6(952), 952–960.